Biointerface Research in Applied Chemistry
Open-Access Journal (ISSN: 2069-5837)

Article
Volume 16, Issue 1, 2026, 21
https://doi.org/10.33263/BRIAC161.021

Computational Neuroinformatics Study of Monomeric Flavans from Superfoods as Potential ACOX1 Modulators in Cerebral Ischemia–Reperfusion Injury

Niranjan Kumar Raghupathi [1], Haja Nazeer Ahamed [1,*], Irfan Navabshan [1]

[1] Crescent School of Pharmacy, B. S. Abdur Rahman Crescent Institute of Science and Technology, Seethakathi Trust, GST Road, Vandalur, Chennai 600048
* Correspondence: haja@crescent.education;

Received: 13.08.2025; Accepted: 28.10.2025; Published: 15.02.2026

Abstract: Cerebral ischemia–reperfusion injury (CIRI) triggers oxidative stress and neuronal damage, wherein modulation of peroxisomal lipid metabolism may confer neuroprotection. This study explores the potential of monomeric flavans from selected superfoods to target human Acyl-CoA oxidase 1 (ACOX1), a key enzyme in fatty acid β-oxidation associated with oxidative neuronal injury. Bioactive small molecules retrieved from the IMPPAT and OSADHI databases were screened using network pharmacology to identify CIRI-related gene targets. Molecular docking, MMGBSA binding energy evaluation, and 100 ns molecular dynamics simulations were conducted employing Schrödinger Glide and Desmond modules. Gene Ontology (GO) and KEGG enrichment analyses revealed involvement of lipid metabolism and oxidative stress pathways. Among the screened phytochemicals, Rutin and Chlorogenic acid demonstrated the highest binding affinities toward ACOX1 with docking scores of -12.18 ± 0.23 and -8.91 ± 0.12, and MMGBSA free energies of −44.73 and −38.76 kcal/mol, respectively. Molecular dynamics analysis indicated high structural stability of the Rutin–ACOX1 complex (RMSD ≈ 2.4 Å), while Chlorogenic acid exhibited moderate flexibility (RMSD ≈ 5.4 Å). Interactions with ACOX1 residues GLN569, ASN570, and SER568 suggested a stabilizing role in peroxisomal redox regulation. These findings highlight Rutin and Chlorogenic acid as promising natural modulators of ACOX1, supporting further mechanistic and experimental validation for their neuroprotective efficacy against ischemic brain injury.

Keywords: ACOX1; cerebral ischemia-reperfusion; molecular modeling; super foods; monomeric flavans.

1. Introduction

Cerebral ischemia–reperfusion injury (CIRI) occurs when blood flow to the brain is temporarily halted and then restored, triggering a cascade of oxidative stress, inflammation, and neuronal death. The restoration of oxygen and nutrients, while essential for survival, paradoxically intensifies the production of reactive oxygen species (ROS), disrupts mitochondrial function, alters lipid metabolism, and compromises neuronal membrane integrity. The cumulative impact of these processes leads to neuronal apoptosis, edema, and long-term neurological impairment [1,2]. Natural polyphenolic compounds are known to modulate oxidative and inflammatory pathways that contribute to cerebral injury. Superfoods,

which are rich in bioactive flavonoids and phenolic acids, have shown potential to counteract oxidative stress and protect the brain. Among these phytochemicals, compounds such as Rutin, Quercetin, and Chlorogenic acid are of particular interest due to their potent antioxidant capacities and reported ability to modulate neuronal survival mechanisms.

Current research focuses on identifying strategies to enhance the beneficial effects of reperfusion while mitigating its harmful consequences [3-5]. Therapeutic approaches such as antioxidants, anti-inflammatory agents, and other neuroprotective drugs have shown promise in experimental models. Several plant-based superfoods have shown promising neuroprotective effects against cerebral ischemia and reperfusion (I/R) injury, owing to their pleiotropic, polyvalent composition of small bioactive compounds. For example, Ficus carica, also known as fig fruit, is enriched with bioactive flavonoids and phenolic acids that exhibit strong antioxidant, anti-inflammatory, and neuroprotective properties [6]. Crocus sativus (Saffron) contains crocin and safranal [7], which have been shown to attenuate ischemia-induced brain injury in a rat model [8] and to confer neuroprotective effects in ischemic stroke patients in randomised [9] clinical trials. Punica granatum (Pomegranate) is abundant in bioactive polyphenols, particularly ellagic acid and punicalagin [10]. These polyphenols not only scavenge free radical production during ischemic insults [11] but also prevent the exacerbation of neuron damage during the reperfusion cascade. Phoenix dactylifera (Date palm) is known for its flavonoid and tannin content, contributing to its neuroprotective, anti-inflammatory, and anti-apoptotic effects [12]. In recent years, bioactive compounds from plant-based superfoods have attracted scientific attention for their potential to counteract oxidative stress and promote neuronal survival. These foods contain multifunctional phytochemicals capable of modulating inflammatory and redox balance, offering an integrative neuroprotective effect. Representative examples include Ficus carica (source of rutin and polyphenols known for antioxidative and anti-inflammatory potential), Phoenix dactylifera (rich in Chlorogenic acid, flavonoids, and tannins with reported anti-apoptotic effects), and Murraya koenigii (a source of carbazole alkaloids and quercetin, shown to regulate oxidative stress and cytokine release) [13–15]. These biomolecules not only attenuate free radical formation but also enhance mitochondrial function and neuronal survival signaling in ischemic models [16–18]. Collectively, polyphenolic superfoods represent promising nutraceutical interventions for mitigating ischemic brain injury [19–21].

Emerging evidence indicates that peroxisomal enzymes play a role in neuroprotection under hypoxic conditions. Among them, human Acyl-CoA oxidase 1 (ACOX1) plays a central role in peroxisomal β-oxidation of very-long-chain fatty acids (VLCFAs), generating hydrogen peroxide as a physiological byproduct [22-24]. Proper ACOX1 function is crucial for neuronal lipid homeostasis and redox regulation. However, its dysregulation increases ROS production, disrupts fatty acid metabolism, and triggers neuroinflammatory cascades associated with conditions such as Alzheimer's disease and multiple sclerosis.[25] Multi-omics investigations and transcriptome analyses have validated reduced ACOX1 expression in ischemic brain and small vessel disease models, linking enzyme dysfunction to inflammasome activation (NF-κB, NLRP3) and mitochondrial stress [26–30]. Consequently, ACOX1 has been recognized as a potential therapeutic target for controlling oxidative stress and lipid metabolic imbalance during CIRI.

Considering its central regulatory role, the present work explores small bioactive molecules from selected superfoods as natural modulators of ACOX1 to counter CIRI-related oxidative neuronal injury. A hybrid computational approach integrating network

pharmacology, molecular docking, MMGBSA binding energy estimation, and molecular dynamics (MD) simulation was employed to identify and validate ACOX1-targeted compounds. Furthermore, Gene Ontology (GO) and KEGG enrichment analyses were performed to elucidate the biological and metabolic pathways associated with ACOX1 regulation

2. Materials and Methods

2.1. Computational methods.

The workflow was executed using specialized software tools optimized for its specific analytical process. The STRING database (version 11.5) was employed for constructing protein–protein interaction (PPI) networks to identify core ischemia–reperfusion (CIRI) targets associated with ACOX1 function. The resulting network visualization and hub-node ranking were performed via Cytoscape (version 3.9.1). Molecular docking was conducted using Schrödinger's Maestro platform (version 2023-1), where the Glide module was utilized in Standard Precision (SP) mode to predict key ligand-receptor interactions. The top-scoring poses from Glide were re-evaluated using Prime MMGBSA to estimate ΔGbind values and refine docking accuracy. Subsequently,[31] Desmond MD simulation software (version 7.6) was applied to examine the long-term stability of protein–ligand complexes under dynamic physiological conditions.

2.2. Collection of small bioactive molecules from indian medicinal plants databases.

The superfoods derived from small bioactive molecules were collected using the following Indian Medicinal Plant databases. The Indian Medicinal Plants, Phytochemistry and Therapeutics Database 2.0 (IMPPAT; https://cb.imsc.res.in/imppat/) and the Online Structural and Analytical Based Database for herbs of India (OSADHI; https://neist.res.in/osadhi/) were used to search for and collect small bioactive molecules from superfoods [32]. The bioactive small molecules were chosen based on the ADMT and toxicological profile, based on the drug-GSK4/400 rule = Passed; Pfizer 3/75 rule = passed; and Weighted quantitative estimate of drug-likeness QEDw > 0.5 score = 1 and ≠ 0.

2.3. Collection of brain ischemic gene targets.

Gene databases such as OMIM (https://www.omim.org/) and Gene Cards (https://www.genecards.org/) retrieve genes. Disease-specific keywords such as "Cerebral Ischemia" and "Ischemic Stroke" were used to identify relevant genes. Genes can be found by searching for disease-related phrases in OMIM, and their functions, molecular mechanisms, and disease associations can be extracted. GeneCards helps validate data by cross-referencing it across various databases and by reviewing primary literature to confirm gene-disease associations.

2.4. PPI interaction analyses.

For the protein-protein interaction network of target gene analyses, the genes were submitted to the STRING database (https://string-db.org/) v11.5 with the species set at "Homo Sapiens". A co-expression pattern threshold of >0.7 was applied to screen the data. After clustering, the network was analysed using Cytoscape 3.9.1. (https://cytoscape.org/) to

construct the regulatory network. The topological parameters of closeness centrality (CC) [33] were screened using the CytoHubba 0.1 plugin to rank target proteins based on their mutations.

2.5. GO enrichment analysis.

In the enrichment analysis, candidate target genes related to CI-RI were evaluated for significant enrichment in specific biological processes, molecular functions, or cellular components using resources such as the Gene Ontology (GO) database (https://geneontology.org/) and Kyoto Encyclopaedia of Genes and Genomes (KEGG) pathways (https://www.kegg.jp/). STRING assesses GO terms across three categories: Biological Process (BP), which describes the biological events associated with the proteins; Molecular Function (MF), which defines the molecular activities the proteins perform; KEGG pathway enrichments and Tissue analysis to understand the biological relevance of their gene/protein set by identifying key processes.

2.5.1. Protein and ligand preparation.

The structure was downloaded from the Protein Data Bank [PDB 7Q84]. Using the protein preparation workflow, the first step was preprocessing, which fills missing residues and loops within the protein model system and optimizes H-bond assignments using PROKA's optimization states. Furthermore, the minimization and deletion of water [34] of ACOX1. For the ligand preparation, the Lig Prep tool was used to correct protonation state and stereochemistry. Further quick energy minimization was performed to optimize the ligands' geometry and relieve steric clashes. Additionally, assign the appropriate force field (OPLS4) and calculate the partial charges, ensuring that the ligand is adequately represented for subsequent docking studies [35].

2.5.2. Binding site detection, grid generation.

Binding site detection and grid generation in Schrödinger, carried out by importing the protein structure into Maestro and using the ligand site as the binding site, proceed to set up the grid by selecting the desired site and defining the grid parameters, including the size and spacing of the grid points [36]. Generate the grid using the Glide tool with x = 7.06, y = -6.15, and Z = 13.89, and a radius of 20, which prepares the area for subsequent docking studies by calculating potential interaction energies for ligands. Finally, review the grid setup to ensure it aligns with the identified binding site, then save the configuration for use in docking.

2.5.3. SAR studies and docking.

The ligand data sets were assessed the SAR studies through esmitates the binding affinity alternatively ligand based approach of 2D QSAR fingerprints of catechol group Substituents, steric tolerance are visualized analogue and further more Qikpro Π-π Stacking, Hydrophobic Interactions, Electrostatic Interactions, and hydrogen bonding and then imported into for docking using Schrödinger's Glide in Extra Precision mode top 1 poses saved per molecule [37]. Then, set the docking parameters, including the scoring function and any necessary constraints. RMSD < 2.0 Å and scoring consistency within 0.5 kcal/mol. After configuring the docking options, Glide is allowed to generate and rank poses of the ligand based on their binding affinities [38]. Once the docking run is complete, analyse the results by reviewing the top-ranked poses and examining the binding interactions.

2.5.4. Molecular mechanics generalized born surface area (MMGBSA).

To perform MM-GBSA (Molecular Mechanics Generalized Born Surface Area) calculations, start by preparing the protein-ligand complex and ensuring that both components are properly optimized and solvated. Use the MM-GBSA method to calculate the binding free energy by evaluating the energy contributions from the molecular mechanics potential, the generalized Born solvent model, and the surface area effects [39]. This involves calculating the energies of the ligand, the protein, and the complex, along with the solvent contribution. Finally, analyze the results to obtain insights into binding affinity, considering both the calculated binding energies and the contributions from various energy components to understand the interactions.

2.6. MD simulation.

For MD simulation studies, the complex of ACOX1 with Rutin and a separate complex of Cholinergic acid were used, and the system utilized the preset H2O SPC solvent model, employing an orthorhombic box as the boundary condition with an initial buffer box size estimated at a = 10.0 Å. B 10.0 Å, c = 10.0 Å. The complex protein's surface occupancy was considered to minimise the final volume, and Na^+, Cl^- ions were added to neutralize the mixture. The solvated model water [SPC] underwent a molecular dynamics simulation, set to run for 100 ns with a trajectory recording interval of 100 PS and an energy cutoff of 1.2 [40]. The simulation was conducted in the NPT ensemble, generating 1000 frames at 300 K temperature and 1.01325 bar pressure. The model was equilibrated before simulation initiation. At the end of the simulation, the interaction diagram module was used to analyze interactions during the simulation and calculate torsion values of the complex over a 100 ns time scale [41]. Additionally, RMSD, RMSF, protein-ligand contacts, ligand-protein interaction map, and Heat map were calculated to assess structural stability and fluctuations. Convergence of the simulation was verified by analyzing Root Mean Square Deviation (RMSD), Root Mean Square Fluctuation (RMSF), and potential energy profiles across the 100 ns trajectory. Stability was confirmed when RMSD values plateaued after approximately 30 ns, and potential energy fluctuations remained below 5%. These observations indicated that equilibrium had been achieved and that the conformations sampled during the latter half of the trajectory accurately represented the stable ligand–ACOX1 binding state

3. Results and Discussion

3.1. PPI interaction analyses.

The computational analysis identified a putative neuroprotective effect of small molecules derived from superfoods on neuronal cell membrane proteins, such as Acyl-CoA oxidase 1 (ACOX1), in an in-silico study. There are 64 bioactive small molecules obtained from six different superfoods. Furthermore, five small bioactive molecules, namely Caffeic acid (IMPHY011933), Rutin (IMPHY015047), Quercetin (IMPHY004619), Luteolin (IMPHY004660), and Chlorogenic Acid (IMPHY011844), were chosen for docking studies. Using the Gene database [42], Figure 1a represents genomic targets for cerebral ischemia and reperfusion injury. The Genomic database retrieved 50 target genes corresponding to CI-RI. Following protein target clustering network analysis, a total of 50 genes were found at the intersection. The genes represented in red colour, as per CYTOHUBBA, showed a greater

mutation (Figure 1b). Furthermore, 5 genes were chosen from CYTOHUBBA prediction on the parameters DC and CC of the genes involved.

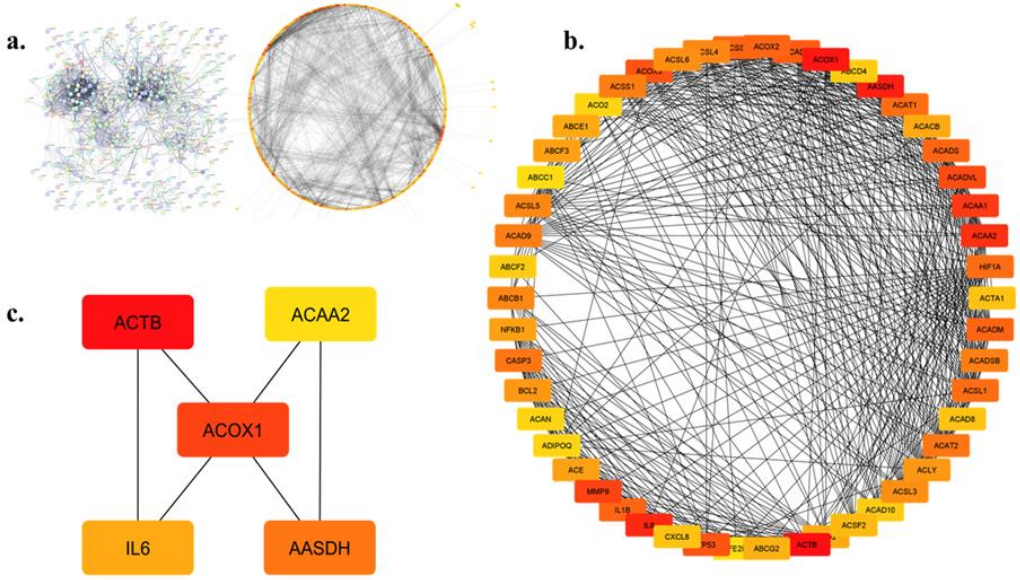

Figure 1. (a) Strings PPI- network interaction of Cerebral Ischemia and Ischemic Stroke; **(b)** PPI- network Interaction closeness region; **(c)** Target identified the interaction of Cerebral ischemia reperfusion injury.

The identified genes are ACOX1, including ACTB, AASDH, ACAA2, and IL6 (Figure 1c), suggesting a pivotal role in cerebral ischemia and reperfusion-induced neuronal injury. In this study, screening results from disease databases also showed that the ACOX1 protein was closely associated with CI-RI (the candidate target gene ranked first; Figure 1c). Therefore, we have identified ACOX1 as the target gene for the follow-up study. Further gene ontology analysis of biological and molecular functions indicates that the glutamatergic pathway is involved through glutamate receptors in cortical and subcortical brain regions.

The tissue enrichment analysis highlights specific tissues, cell types, and receptor families associated with the gene sets. The bar graph demonstrates the extent of enrichment across various tissues and cellular environments. Notably, the brain and its associated regions, including the prefrontal cortex, forebrain, cerebral hemispheres, and hippocampus, show significant enrichment, underscoring the importance of neural tissues in biological contexts.(Figure 3) Other enriched cell types include interneurons, synovial fibroblasts, and cerebral cortical neurons, suggesting specialized cellular involvement. The pie chart provides a classification of receptor families enriched within the dataset. The Major Facilitator Superfamily accounts for the largest proportion (43%), followed by receptor family ligand-binding regions (30%) and sodium-electrolyte symporter families (11%). These receptor families reflect the molecular functions and interactions crucial to the observed enrichment in neural and other tissue types.(Figure 2b) This tissue-specific, receptor-family-focused enrichment analysis underscores the functional relevance of the genes to neural and synaptic activity while also indicating potential roles in broader physiological contexts, such as immune or connective tissues. It has been documented that glutamate receptor-mediated excitatory synaptic pathways are associated with impaired brain metabolism, oxidative stress [43], inflammation, and cytoskeletal damage [44] in ischemia and reperfusion-induced neuronal injury. Co-localisation of ACOX1 with the PPARα receptor in the ventral pallidum and globus pallidus helps control cholinergic neurotransmission through the peroxisomal β-oxidation pathway by affecting Acyl-CoA units necessary for acetylcholine synthesis [45].

The ubiquitous role of PPAR alpha in the CNS has been established [46]. In particular, the regulation of brain lipid metabolism and reactive oxygen/nitrogen species metabolism through associated genes, such as ACOX1, superoxide dismutase (SOD1), and Catalase (CAT), has been shown in experimental rat models [47]. Further supporting this, recent investigations on microglial and oligodendrocyte cell lines lacking the peroxisomal ACOX1 gene show increased reactive oxygen species (ROS) and nitrogen species (NO) [48]. (Figure 2a) Genetic ontology analysis concerning biological and molecular function enrichment suggests that the involvement of ionotropic glutamate receptors mediates signalling with glutamatergic synapses. The false discovery rate (FDR) value is extremely low (FDR< 1 x $10e^{-36}$), suggesting high statistical confidence and reliability, with larger gene counts correlating to prominent enrichment. Further, the KEGG pathway enrichment analysis overlapped with GO ontology enrichment, revealing significant enrichment in pathways such as the glutamatergic synapse and neuroactive ligand-receptor interaction. The ionotropic glutamate-regulated Ca^{2+} channel receptors play a role in cerebral ischemia and reperfusion injury [49]. The phosphorylation of NMDA receptor subunits by glutamate at synaptic and extrasynaptic sites and redistribution within the selectively vulnerable neuron population (SVN) have been documented in a rat model of ischemic stroke [50]. Recent experimental evidence highlights the importance of ACOX1 upregulation-mediated autophagy in colorectal cancer cells via ROS/mTOR cell signaling pathways [51]. On the contrary, the ACOX1 downregulation in neuroglial and neuroblastoma cell lines following enterovirus 71 exposure induced neuronal apoptosis and autophagy [52].

3.2. GO enrichment analysis.

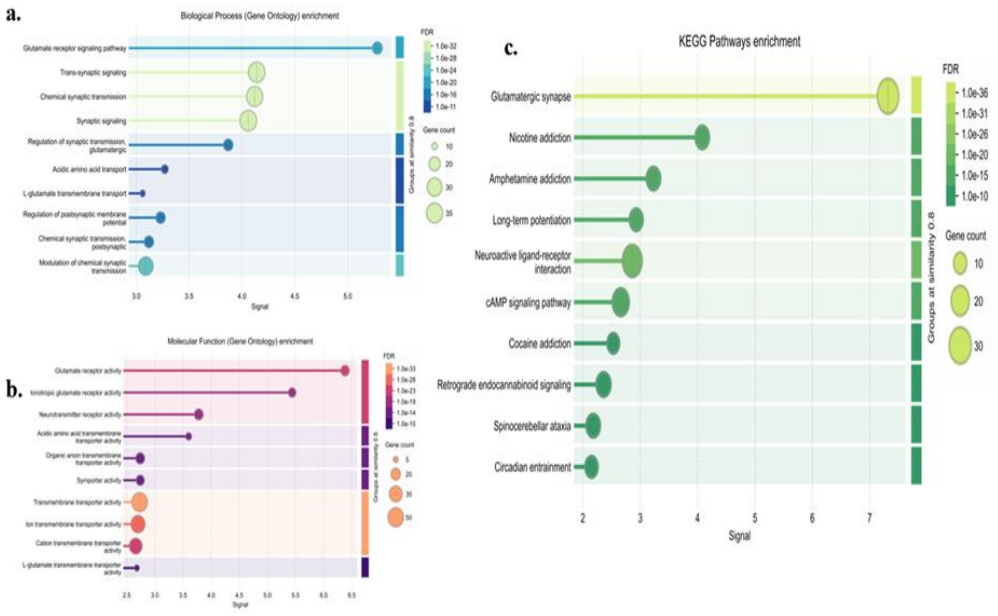

Figure 2. (a) Biological process of gene ontology; **(b)** Molecular function associated with Ischemia and Reperfusion Injury; **(c)** KEGG pathway analysis.

Gene Ontology (GO) and KEGG enrichment analyses indicated that ACOX1 and its associated genes are primarily involved in regulating oxidative balance and lipid metabolism in neuronal systems affected by ischemia-reperfusion [53]. The main biological processes identified included fatty acid β-oxidation, oxidoreductase activity, and responses to reactive oxygen species, indicating the enzyme's fundamental involvement in controlling oxidative

damage. Enrichment within peroxisomal and mitochondrial components further supports ACOX1's contribution to lipid degradation and energy homeostasis in neurons. At the functional level, terms such as acyl-CoA oxidase function and hydrogen peroxide detoxification confirmed its significance in maintaining cellular redox stability [54]. The KEGG pathway mapping revealed four core networks: (1) Peroxisome signaling, which assists in fatty acid catabolism and ROS neutralization; (2) PPAR signaling, important for lipid regulation and anti-inflammatory defense; (3) Glutathione metabolism, critical for redox buffering during oxidative insults; and (4) MAPK/NF-κB signaling cascades, linked to inflammatory and oxidative stress responses in neurons. (Figure 2c)Together, these enriched processes demonstrate that ACOX1 operates at the intersection of lipid oxidation, energy regulation, and oxidative defense, supporting its potential as a therapeutic target to mitigate neuronal damage following ischemia-reperfusion [55].

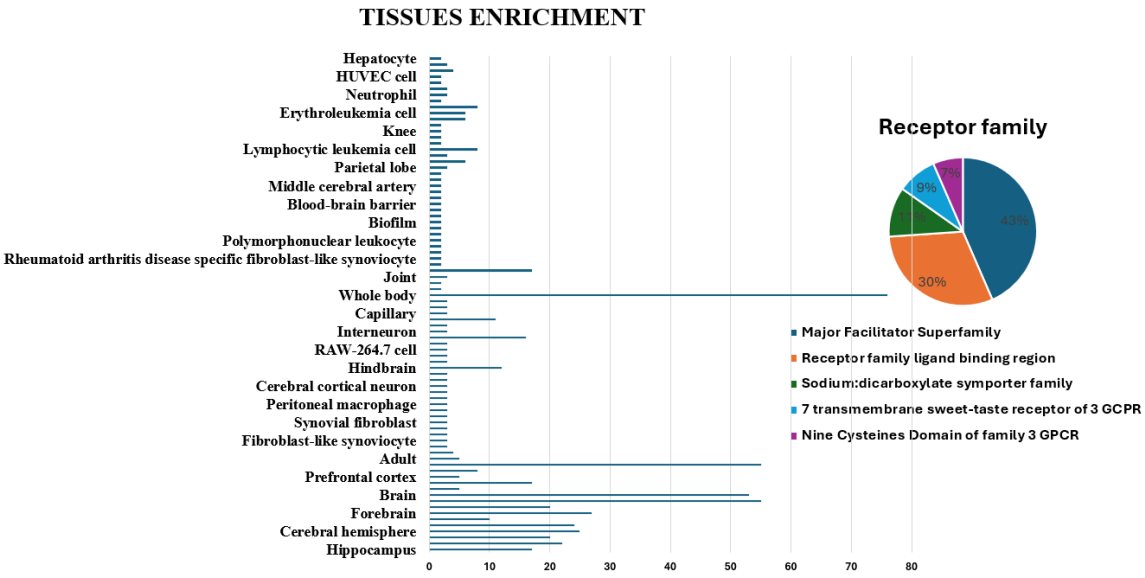

Figure 3. Represents the tissue enrichment analysis of cerebral ischemia and reperfusion injury.

3.3. SAR studies and docking.

The target protein ACOX1, as shown in Figure 4a, exhibits a well-defined binding pocket with strong ligand-binding capacity. The ligands establish multiple stabilising interactions, indicating strong binding affinity and specificity. The protein-ligand binding affinities of 5 small molecules were established using interactive Venn diagrams (Figure 4b). It is observed that the catechol nucleus monomeric 3-flavanol is completely bound to the inside cavity of ACOX1. Structure-Activity Relationship (SAR) analysis (Figure 4c) represents the molecular structures of ligands. The presence of hydroxyl (-OH) and carboxyl (-COOH) groups contributes to hydrogen bonding, while conjugated ring systems enhance π-π stacking interactions. Hydrophobic interactions are primarily observed in fused ring systems, where nonpolar regions of the ligands interact with hydrophobic pockets. Electrostatic interactions arise from charged or polar functional groups, such as carboxyl and hydroxyl groups, which form ionic or dipole interactions with complementary residues [56]. Hydrogen bonding is a crucial factor in ligand binding, with hydroxyl, carbonyl, and glycosidic groups forming strong interactions with polar amino acids of the protein target. The structure active relationship indicates that the flavonoid glycoside and flavanol catechol moiety of the B ring, 2,3 double bond conjugating with 4-oxo group in the C ring in the flavonols, hydroxyl groups at the 3 and

5 positions of the A and C ring exhibit the strongest binding potential, attributed to their extensive π-π stacking, hydrophobic interactions, and multiple hydrogen bond donors and acceptors. These properties enhance their stability and affinity toward the ACOX1 protein (Table 1). On the contrary, phenyl acrylic acid and phenolic glycoside show moderate binding due to fewer π-π stacking interactions and limited hydrophobic interactions.

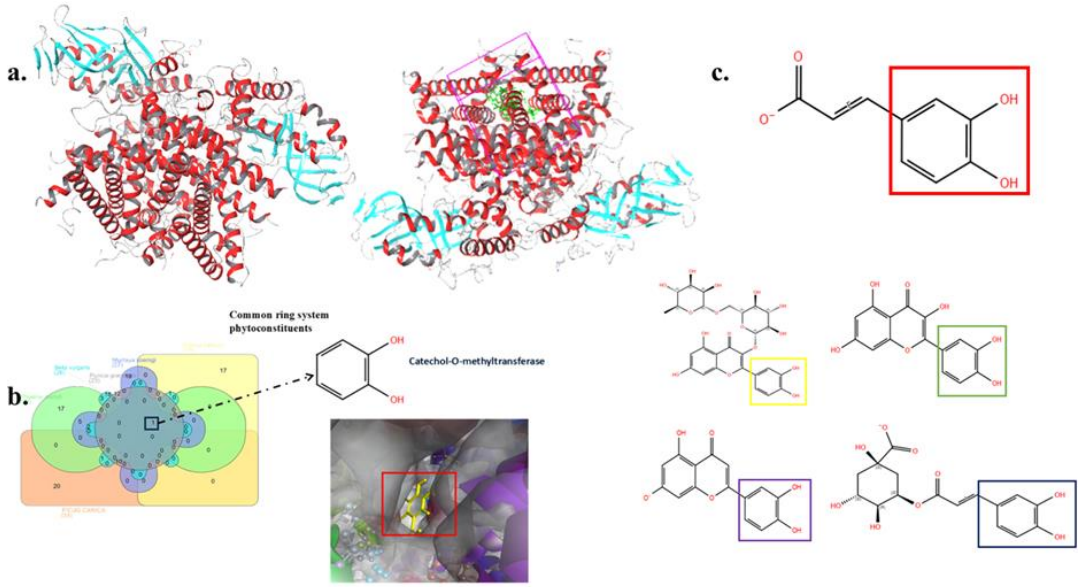

Figure 4. (a) Secondary Structure of ACOX; **(b)** Phytoconstituents Crocus sativus, Ficus carica, Beta vulgaris, Phoenix dactylifera, Murraya koenigii analysis phytoconstituents; **(c)** SAR selected COMT Phytoconstituents Analysis of Super foods.

While demonstrating moderate binding efficiency, Isoflavone lacks strong electrostatic interactions, making it less favourable than flavonoid glycosides and flavonols. The observed SAR overlaps with the previous reports on the neuroprotective potential of quercetin and rutin in a rat hippocampal CA1 neuron degenerative model following repeated bilateral common carotid artery occlusion induced cerebral ischemic injury model [57].

Table 1. SAR Analysis of small molecules from super foods

Structure	Core Structure	Key functional groups	II-π Stacking	Hydrophobic Interactions	Electrostatic Interactions	Hydrogen Bonding
Caffeic acid IMPHY011933	Phenyl acrylic scid	Hydroxyl (-OH), carboxyl (-COO⁻)	Moderate (Benzene ring)	Present (Aromatic ring)	Weak (Carboxylate group)	Strong (carboxyl and hydroxyl groups)
Rutin IMPHY015047	Flavonoid glycoside	Multiple hydroxyl (-OH), ether (-O-)	Strong (Multiple benzene rings)	Present (Fused rings)	Moderate (-OH and carbonyl)	Strong (hydroxyls and glycosidic oxygen)
Quercetin (IMPHY004619)	Flavonol	Hydroxyl (-OH), carbonyl (-C=O)	Strong (planar conjugated system)	Strong (hydrophobic core)	Weak (carbonyl oxygen)	Strong (hydroxyls and carbonyl oxygen)
Luteolin IMPHY004660	Isoflavone	Hydroxyl (-OH), carbonyl (-C=O), ether (-O-)	Strong (phenyl + Isoflavone core)	Moderate (benzene and fused rings)	Weak (few charged groups)	Strong (hydroxyl + carbonyl)
Chlorogenic acid IMPHY011844	Phenolic Glycoside	Hydroxyl (-OH), ester (-COO-), sugar moiety	Moderate (aromatic ring)	Present (benzene core)	Moderate (ester and hydroxyl)	Strong (glycosidic oh and carbonyl)

Rutin, a glycosylated form of quercetin, exhibits the strongest binding to ACOX1 among the analyzed ligands. Its polyphenolic structure and sugar residues contribute to a dense interaction network. Key hydrogen bonds are formed with GLN B:569 (2.38 Å), ASN A:570 (2.38 Å), SER A:568 (2.45 Å), GLY B:572 (2.55 Å), and ARG B:525 via a π-interaction at 3.92 Å. These interactions are essential for ligand stabilization in the active site. Hydrophobic

contacts with ILE B:539, ALA B:571, and π–π stacking with TYR A:529 further reinforce the binding. Electrostatic interactions with GLU B:532 and ASP B:526 enhance the overall affinity. The extensive polar and nonpolar interactions support rutin's potential for modulating oxidative stress pathways.

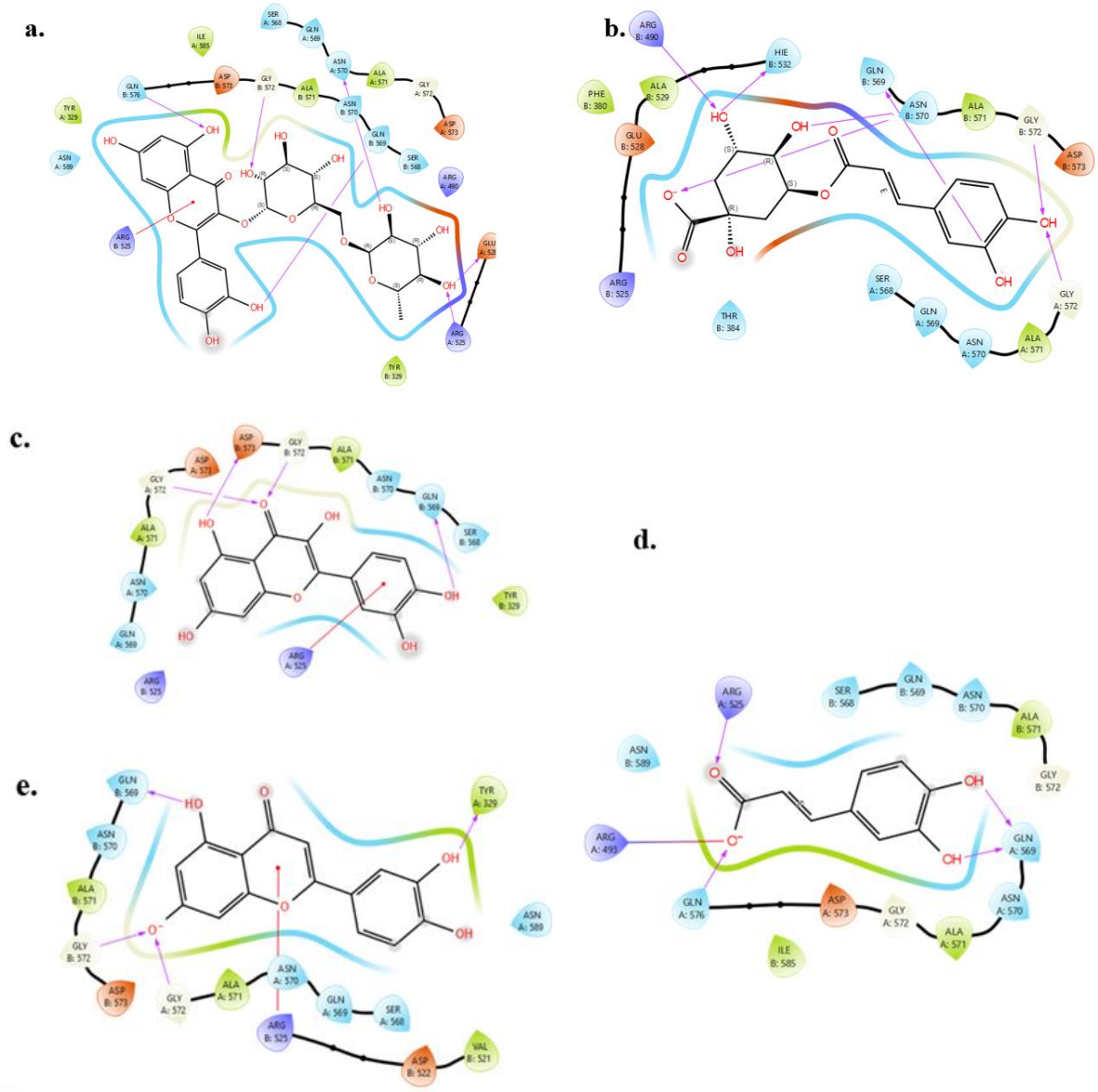

Figure 5. Interaction analysis of ACOX1 with **(a)** Rutin; **(b)** Chlorogenic acid; **(c).** Quercetin; **(d)** Caffeic acid; **(e)** Luteolin.

These interactions are depicted in Figure 5a. Chlorogenic acid, a phenolic compound with a simpler framework, demonstrates effective yet moderate binding. It forms hydrogen bonds with GLN B:569 (2.13 Å), ASN A:570 (2.37 Å), SER A:568 (2.64 Å), and ASP B:528 (2.84 Å), which contribute to ligand stability through polar contacts. A π-interaction with ARG B:525 at 5.04 Å supports binding orientation. Hydrophobic interactions with ALA B:571 and PHE B:380 (aromatic stacking) stabilize the compound within the hydrophobic pocket. Electrostatic contacts with ARG B:490 and ASP B:528 are critical for anchoring the ligand. While not as extensive as rutin, the balanced combination of polar and hydrophobic interactions allows Chlorogenic acid to exhibit selective and stable binding, as shown in Figures 5b and 6b.

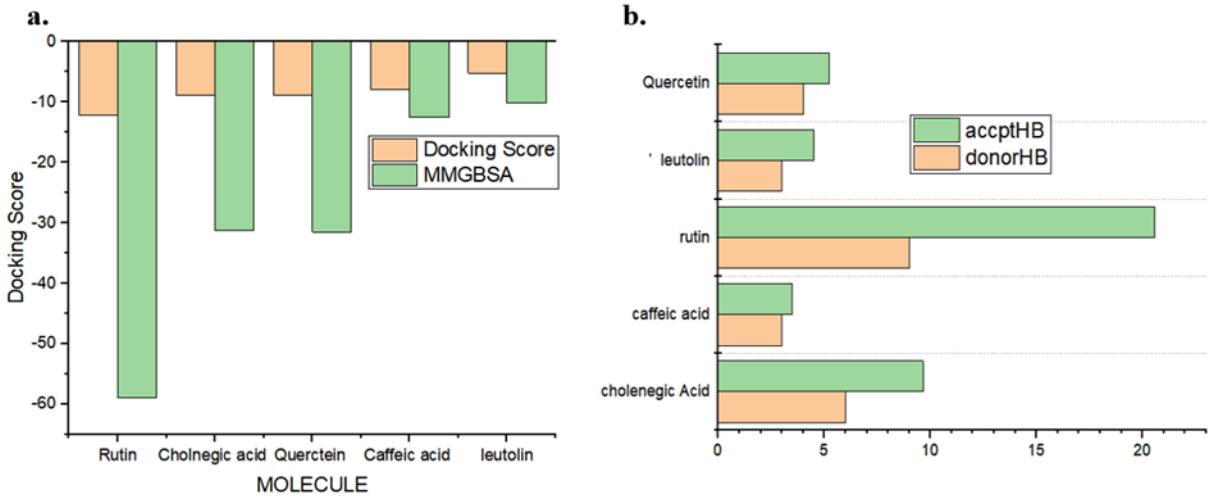

Figure 6. Acyl-CoA oxidase **(a)** Docking and MMGBS bar Graph; **(b)** Hydrogen bond acceptor and donor.

Quercetin presents a highly stable binding profile with ACOX1, as indicated by its docking score and MMGBSA energy. The ligand forms hydrogen bonds with GLN B:569 (2.34 Å), ASN A:570 (2.25 Å), SER A:568 (2.53 Å), and GLY B:572 (1.98 Å). A π-cation interaction with ARG B:525 at 6.04 Å significantly contributes to the binding affinity. Hydrophobic contacts with ALA B:571, ILE B:539, and TYR A:529 stabilize the complex. Electrostatic interactions with ARG B:525 support further anchoring, especially through the ligand's hydroxyl groups. These interactions collectively reflect a robust ligand-receptor complex, as illustrated in Figures 5c and 6a. Caffeic acid demonstrates moderate binding strength, attributed to fewer but specific interactions. Hydrogen bonds are observed with GLN A:569 (3.22 Å), ASN A:570 (3.48 Å), and SER B:568 (3.55 Å), which help orient the ligand in the binding site. It shows a π-interaction with ARG B:525 at 5.34 Å. Hydrophobic interactions with ALA B:571, ILE B:585, and GLY B:572 provide support but are less significant compared to other ligands. Electrostatic contacts with ARG A:489 and ASP A:573 further stabilize the compound, although the overall MMGBSA energy suggests a lower binding affinity. These results are reflected in Figures 5d and 6a. Luteolin, a flavonoid compound, exhibits moderate to low binding affinity to ACOX1.

Table 2. Represents the values of binding free energy, predicted inhibition constant, MMGBSA, and the number of hydrophobic and hydrophilic interactions of super foods' small molecules.

Ligand	Docking score mean ± SD (Kcal/mol)	MMGBSA energy (Kcal/mol)	Ki (nm)	π– interaction residue with distance	Key hydrogen bonding residues with distance	Key hydrophobic residues	Key electrostatic interactions
Rutin	-12.18 ± 0.23	-44.73	1.28	ARG B:525- 3.92 Å	GLN B:569 - 2.38 Å SER A:568 - 2.19 Å ASN A:570 - 2.38 Å GLY B:572 - 2.55 Å	ILE B:539, ALA B:571, TYR A:529	GLU B:532, ARG B:526
Chlorogenic Acid	-8.91 ± 0.12	-38.76	281.32	-	GLN B:569 - 2.13 Å ASN A:570 -2.37 Å SER A:568 - 2.64 Å ASP B:525 -6.28 Å	PHE B:380, ALA B:571	ARG B:490, ASP B:528
Quercetin	-8.78 ± 0.17	-31.47	326.92	ARG B:525 -6.04 Å	GLN B:569 -2.67 Å SER A:568 - 5.24 Å ASN A:570 -2.64 Å GLY B:572 -1.98 Å	ALA B:571, TYR A:529, ILE B:539	ARG B:525
Caffeic acid	-7.83 ± 0.12	-12.50	1539.59	-	GLN A:569 - 3.22 Å ASN A:570 - 3.84 Å SER B:568 - 5.35 Å	ALA B:571, ILE B:585, GLY B:572	ARG A:489, ASP A:573

Ligand	Docking score mean ± SD (Kcal/mol)	MMGBSA energy (Kcal/mol)	Ki (nm)	π– interaction residue with distance	Key hydrogen bonding residues with distance	Key hydrophobic residues	Key electrostatic interactions
Luteolin	-5.17 ± 0.07	-10.13	147,544.03	ARG B:525 -3.75A	GLN A:569 -3.42 Å ASN A:570 - 3.59 Å SER A:568 - 2.85 Å	ALA B:571, GLY B:572, TYR A:529	ARG A:525

It forms hydrogen bonds with GLN A:569 (3.42 Å), ASN A:570 (3.59 Å), and SER A:568 (2.85 Å), along with a π-interaction with ARG B:525 at 3.75 Å. Hydrophobic interactions with ALA B:571 and TYR A:529 assist in maintaining the ligand within the active site. Electrostatic stabilization is provided by ARG B:525. Despite its lower MMGBSA energy compared to other ligands (Table 2), Luteolin's balanced set of polar and hydrophobic contacts provides a basis for stable, albeit weaker, receptor binding. These interactions are highlighted in Figures 5e and 6c. The nature of the cavity and hydrogen bond donor (pink) and Acceptor (green) profile is shown during the binding in Figure 7.

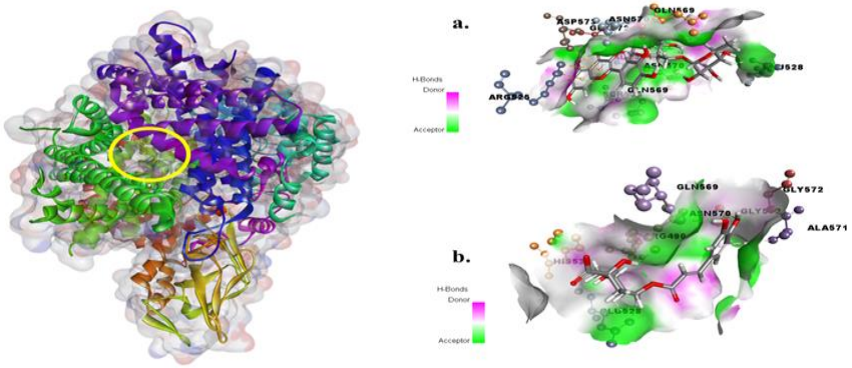

Figure 7. Secondary structure of protein with docked molecules. **(a,b)** Cavity binding of the molecules.

3.4. MD simulation.

The Root Mean Square Deviation (RMSD) is a key indicator of the structural stability of a protein-ligand complex during molecular dynamics simulations.

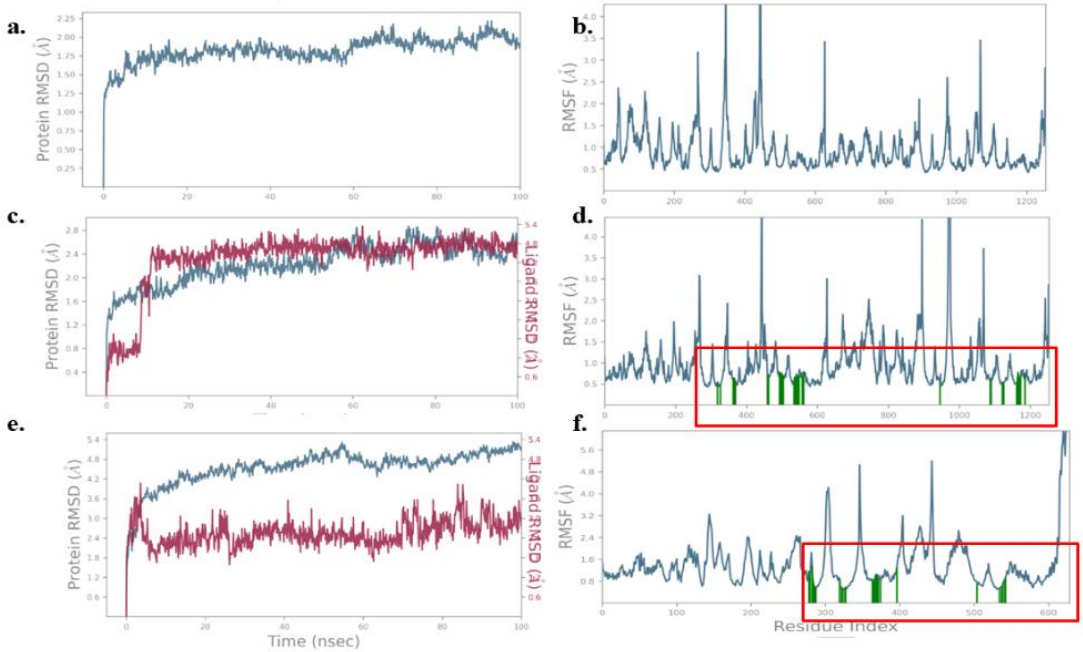

Figure 8. (a) RMSD of ACOX1 protein; **(b)** RMSF of acox1; **(c)** RMSD complex ACOX1 with rutin; **(d)** RMSF complex ACOX1 with rutin; **(e)** RMSD Complex ACOX1 with cholinergic acid; **(f)** RMSF complex ACOX1 with cholinergic acid.

Fig 8a represents ACOX1, the RMSD stabilizes around 2.0-2.2Å, indicating a well-equilibrated system with minimal structural deviations. This suggests that the protein maintains its native conformation without major conformational shifts. In Figure 8c, rutin exhibits a slightly higher RMSD (~2.4 Å), reflecting some conformational adjustments due to ligand binding. However, the fluctuations remain within the acceptable range, suggesting a stable interaction of rutin with ACOX1. In Figure 8e, Chlorogenic Acid, on the other hand, shows the highest RMSD (~5.4 Å), which indicates significant structural perturbations. This suggests that Chlorogenic Acid may induce more dynamic movements in the protein, potentially leading to conformational instability or weaker ligand binding.

The Root Mean Square Fluctuation (RMSF) highlights the flexibility of different protein residues upon ligand binding—the standard shows minimal fluctuations, indicating that the protein remains stable throughout the simulation. Rutin induces moderate flexibility, particularly in specific residue regions (400–1200) residues (Figure 8d). These fluctuations suggest that rutin interacts with key amino acids, causing local conformational changes while still maintaining overall stability—notably, Chlorogenic acid. Induces much higher fluctuations in the 300–600 residue region (Figure 8f), suggesting that it interacts with flexible loop regions or less stable binding pockets. The binding interactions of the ligands were analysed by measuring key contacts and hydrogen bond distances (in angstroms, Å). Rutin forms strong hydrogen bonds with GLN B:569 (2.8 Å), SER A:568 (3.1 Å), and ASN A:570 (2.6 Å), stabilizing the complex. It also establishes hydrophobic interactions with ALA B:571 (4.2 Å) and TYR A:529 (4.5 Å), contributing to the binding stability. In contrast, Chlorogenic acid forms weaker hydrogen bonds with GLN B:569 (3.4 Å), ASN A:570 (3.8 Å), and THR B:384 (3.7 Å), which may contribute to its higher RMSD and lower stability. Furthermore, electrostatic interactions with ARG A:525 (3.9 Å) provide additional stabilisation for rutin, whereas Chlorogenic Acid exhibits weaker electrostatic stabilisation with ARG A:489 (4.5 Å), leading to higher fluctuations.

3.5. Protein ligand contacts with fraction.

The interaction analysis of the molecular structure of rutin complex amino acids plays a crucial role in stabilising the system through hydrogen bonds, hydrophobic interactions, ionic bonds, and water bridges. ALA_296, CYS_297, and THR_298 exhibit the highest interaction fractions, exceeding 1.0, mainly due to the strong presence of hydrogen bonds and water bridges. SER_294, LYS_295, and LEU_293 show moderate interaction fractions of 0.3-0.6, contributing significantly through hydrogen bonding and water-mediated interactions. Additionally, TYR_565 and ASN_570 display interaction fractions above 0.4, with a combination of hydrogen bonding, water bridges, and some hydrophobic contributions. These residues play a fundamental role in the overall molecular interactions by stabilizing the protein-ligand complex.

The interaction patterns are slightly different, but some key residues remain prominent. LEU_334, GLY_566, and TYR_562 show substantial interaction fractions, primarily engaging in hydrophobic and water-bridged interactions. LYS_330 and PRO_333 contribute with lower interaction fractions near 0.2, primarily forming water bridges. HIS_414, HIS_432, and PHE_392 show minor interaction fractions but still play a role in maintaining structural stability. ALA_384 and TRP_383 contribute significantly to the molecular interactions with noticeable hydrogen bonding and hydrophobic interactions. Overall, this analysis indicates that the second image contains a more balanced interaction distribution, with key residues providing

different stabilizing forces crucial for the molecular complex. It was shown in Figure 9a that ligand contacts ligand through hydrogen bonds and water-mediated interactions.

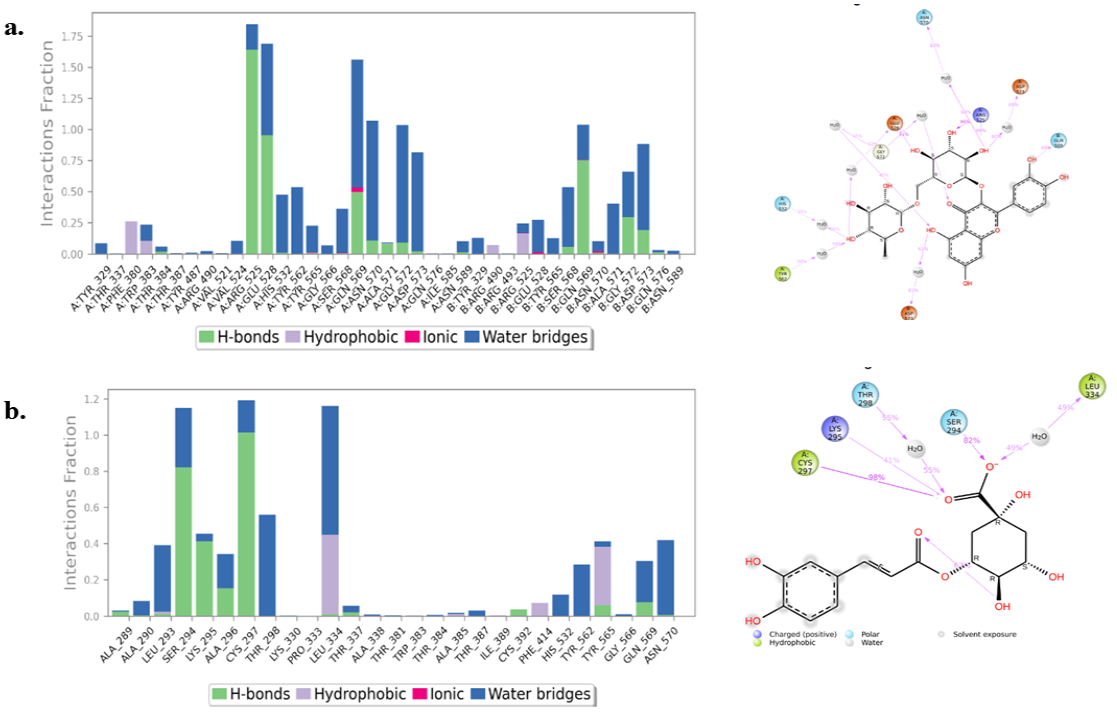

Figure 9. (a) Rutin complex protein ligand contacts; **(b)** Cholinergic acid protein ligand contacts.

Among them, ASN_570 and GLU_428 exhibit the highest interaction percentages at 63%, indicating their strong involvement in molecular stabilization. GLN_569, ASP_572, and ARG_429 interact closely with 60% of the binding energy, contributing significantly to the binding process. Additionally, GLY_572 and TYR_562 show interaction fractions of 50%, while HIS_432 presents a lower but still relevant 39% contribution. These interactions highlight the importance of both direct hydrogen bonding and water-mediated bridges in maintaining the structural integrity of the ligand within its binding site. In Figure 9b, while the cholinergic acid interaction patterns are slightly different, some key residues remain prominent. LEU_334, GLY_566, and TYR_562 show substantial interaction fractions, primarily engaging in hydrophobic and water-bridged interactions. LYS_330 and PRO_333 contribute with lower interaction fractions near 0.2, primarily forming water bridges. HIS_414, HIS_432, and PHE_392 exhibit minor interaction fractions but still contribute to maintaining structural stability. ALA_384 and TRP_383 contribute significantly to the molecular interactions with noticeable hydrogen bonding and hydrophobic interactions. Overall, this analysis indicates that the second image shows a more balanced distribution of interactions, with key residues providing distinct stabilizing interactions. The ligand-protein interaction analysis demonstrates a strong binding affinity mediated by hydrogen bonds, hydrophobic interactions, water bridges, and minimal ionic interactions. The hydrogen bond interactions show significant contributions from SER 294 (82%), CYS 297 (98%), and LYS 295 (98%), indicating a stable and well-anchored ligand within the binding pocket. Additionally, ASN 570 (49%) and THR 298 (55%) also contribute to hydrogen bonding, reinforcing the ligand's stability. Water bridges play a crucial role in stabilizing the ligand, particularly at ALA 296, TYR 565, GLN 569, and ASN 570, forming an extensive hydrogen-bonding network that enhances ligand affinity. The hydrophobic interactions, primarily involving LEU 334 (49%), CYS 297, and THR 298, contribute to the nonpolar stabilization of the ligand, helping to maintain its position within the

binding site. The interaction fraction analysis reveals that water bridges are the dominant interaction type, followed by hydrogen bonds and hydrophobic interactions, while ionic interactions are minimal and do not significantly influence binding stability. Overall, the ligand remains well-stabilized within the binding pocket through a balanced combination of hydrogen bonds (~82–98% contribution), water bridges (~49–55%), and hydrophobic interactions (~49%). This dynamic yet stable interaction network ensures strong molecular recognition, contributing to a favourable and sustained binding mode.

3.6. Heat map analysis.

The heatmaps provide insight into the binding interactions of Rutin (Figure 10a) and Chlorogenic Acid (Figure 10b) with their respective targets over time. In rutin's interaction profile (Figure 10a), residues such as TYR_129, ARG_469, and HIS_532 maintain stable contacts, indicating their roles in forming hydrogen bonds and electrostatic interactions that are crucial for ligand binding. Additionally, VAL_524, LEU_566, and ALA_571 contribute to hydrophobic stabilization, which suggests a relatively rigid binding mode. Some residues, such as THR_384 and TYR_562, exhibit intermittent interactions, potentially enabling conformational flexibility within the binding pocket. These findings indicate that rutin forms a stable complex through a mix of hydrophobic and polar interactions, ensuring effective binding to the target. In contrast, the Chlorogenic Acid binding profile (Figure 10b) highlights the dominance of hydrogen bonding and polar interactions. Residues such as SER_294, THR_298, and ASN_570 are involved in persistent polar interactions, suggesting a binding mode driven by water-mediated hydrogen bonding. CYS_297, LYS_330, and PHE_414 exhibit strong interactions, with CYS_297 playing a crucial role in ligand stability. Unlike Rutin, Chlorogenic Acid appears to interact in a more flexible environment, enabling adaptive binding via transient hydrogen bonding and electrostatic interactions. Comparing both, rutin’s binding is more rigid and hydrophobic, while chlorogenic acid relies more on flexible hydrogen bonding interactions. This suggests that rutin may have a more stable, prolonged interaction, whereas chlorogenic acid may allow dynamic conformational adjustments, depending on the target's structural needs.

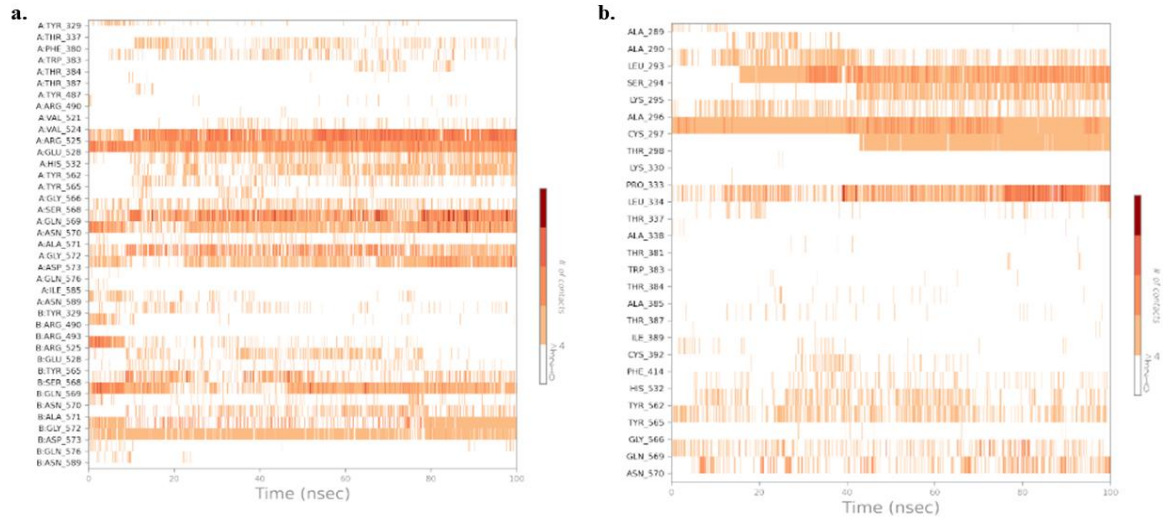

Figure 10. Heat map interaction **(a)** Rutin complex of ACOX1; **(b)** Chlorogenic acid complex.

The combined docking and molecular dynamics analyses provided a comprehensive understanding of how monomeric flavans interact with ACOX1 at the atomic level. Docking

studies revealed that rutin and chlorogenic acid exhibited the strongest binding affinities toward the enzyme's active site, engaging catalytic residues GLN569, ASN570, and SER568 through multiple hydrogen bonds, π–π interactions, and electrostatic contacts. These residues are critical for acyl-CoA oxidation and hydrogen peroxide generation, suggesting that ligand binding could stabilize the catalytic pocket and modulate enzyme activity, thereby minimizing oxidative stress in neuronal cells. The subsequent 100 ns MD simulations reinforced these observations by confirming the persistent stability of the ligand-enzyme complexes under physiological conditions. The rutin–ACOX1 complex maintained an average RMSD of approximately 2.4 Å with minimal residue fluctuations, indicating conformational equilibrium and durable interaction strength. The chlorogenic acid complex exhibited higher RMSD values (~5.4 Å), implying greater flexibility and weaker anchoring within the binding pocket. The dynamic hydrogen-bond profiles obtained during trajectory analysis demonstrated that rutin formed long-lasting contacts with GLN569 and ASN570, preventing local structural displacement. Integrating these parameters highlights a consistent mechanism in which rutin achieves superior stabilization of the ACOX1 active site, enhancing peroxisomal redox homeostasis and potentially reducing ROS production during ischemia–reperfusion stress. These computational findings collectively validate ACOX1 as a redox-modulating target and underscore rutin as a potent lead compound that preserves enzyme structural integrity, a critical factor for neuroprotection.

4. Conclusions

This computational study explored the neuroprotective potential of monomeric flavans, identifying rutin and chlorogenic acid as potent modulators of the peroxisomal enzyme ACOX1. Using integrated network pharmacology, molecular docking, MM-GBSA energy analysis, and molecular dynamics simulations, both compounds demonstrated consistent interactions with critical residues (GLN569, ASN570, and SER568) that regulate ACOX1 enzymatic activity. Rutin displayed particularly stable binding and favorable energy profiles, suggesting a higher potential for therapeutic application in mitigating ischemia-induced oxidative neuronal damage. The novelty of this work lies in establishing ACOX1 as a viable neuroprotective target for cerebral ischemia-reperfusion injury through in silico methods. However, as a limitation, these computational findings require empirical validation. Further investigation using in vitro enzyme assays and in vivo ischemic models is necessary to confirm the predicted efficacy and safety of these compounds.

Additionally, expanding the screening of phytochemicals using high-throughput molecular dynamics and quantum-level simulations could refine lead optimization. Overall, this research contributes to the growing evidence that natural flavonoids from superfoods hold promise as next-generation modulators of lipid metabolism and oxidative stress pathways. By integrating computational pharmacology with molecular insights, this study provides a foundation for future experimental work aimed at developing ACOX1-targeted neuroprotective therapeutics.

Author Contributions

Conceptualization, N.K.G.; methodology, I.N.; formal analysis, I.N.; investigation, H.N.A.; supervision, H.N.A.; writing—original draft preparation, N.K.G.; writing—review and editing,

N.K.G., H.N.A., and I.N. All authors have read and agreed to the published version of the manuscript.

Data Availability Statement

Data available on request from the authors.

Institutional Review Board Statement

Not applicable.

Informed Consent Statement

Not applicable.

Funding

No public funding has been received from any organisation.

Acknowledgement

The authors acknowledge the institute's management for providing the necessary lab facilities for the work.

Conflict of Interest

None declared.

References

1. Li, M.; Tang, H.; Li, Z.; Tang, W. Emerging Treatment Strategies for Cerebral Ischemia–Reperfusion Injury. *Neuroscience* **2022**, *507*, 112–124, https://doi.org/10.1016/j.neuroscience.2022.10.020.
2. Chang, C.; Zhao, Y.; Song, G.; She, K. Resveratrol Protects Hippocampal Neurons against Cerebral Ischemia–Reperfusion Injury via Modulating JAK/ERK/STAT Signaling Pathway in Rats. *J. Neuroimmunol.* **2018**, *315*, 9–14, https://doi.org/10.1016/j.jneuroim.2017.11.015.
3. Jia, L.; Wang, F.; Gu, X.; Weng, Y.; Sheng, M.; Wang, G.; Li, S.; Du, H.; Yu, W. Propofol Postconditioning Attenuates Hippocampus Ischemia–Reperfusion Injury via Modulating JAK2/STAT3 Pathway in Rats after Autogenous Orthotropic Liver Transplantation. *Brain Res.* **2017**, *1657*, 202–207, https://doi.org/10.1016/j.brainres.2016.12.015.
4. Huebner, E.A.; Strittmatter, S.M. Axon Regeneration in the Peripheral and Central Nervous Systems. In Cell Biology of the Axon, Koenig, E., Ed.; Springer Berlin Heidelberg: Berlin, Heidelberg, **2009**; pp. 305-360, https://doi.org/10.1007/400_2009_19.
5. Rehman, M.U.; Wali, A.F.; Ahmad, A.; Shakeel, S.; Rasool, S.; Ali, R.; Rashid, S.M.; Madkhali, H.; Ganaie, M.A.; Khan, R. Neuroprotective Strategies for Neurological Disorders by Natural Products: An Update. *Curr. Neuropharmacol.* **2019**, *17*, 247–267, https://doi.org/10.2174/1570159x16666180911124605.
6. Kumar, R.N.; Ahamed, H.N. Superfoods and Their Impact on Brain Health: A Systematic Review. *Discov. Food* **2025**, *5*, 1, https://doi.org/10.1007/s44187-024-00267-5.
7. Dai, J.; Xiang, Y.; Fu, D.; Xu, L.; Jiang, J.; Xu, J. Ficus carica L. Attenuates Denervated Skeletal Muscle Atrophy via PPARα/NF-κB Pathway. *Front. Physiol.* **2020**, *11*, 580223, https://doi.org/10.3389/fphys.2020.580223.
8. Fan, Y.; Li, Y.; Yang, Y.; Lin, K.; Lin, Q.; Luo, S.; Zhou, X.; Lin, Q.; Zhang, F. Chlorogenic acid promotes angiogenesis and attenuates apoptosis following cerebral ischaemia-reperfusion injury by regulating the PI3K-Akt signalling. *Pharm. Biol.* **2022**, *60*, 1646-1655, https://doi.org/10.1080/13880209.2022.2120161.

9. Azami, S.; Shahriari, Z.; Asgharzade, S.; Farkhondeh, T.; Sadeghi, M.; Ahmadi, F.; Vahedi, M.M.; Forouzanfar, F. Therapeutic potential of saffron (Crocus sativus L.) in ischemia stroke. *Evid.-Based Complementary Altern. Med.* **2021**, *2021*, 6643950, https://doi.org/10.1155/2021/6643950.
10. Abdel-Rahman, R.F.; El Awdan, S.A.; Hegazy, R.R.; Mansour, D.F.; Ogaly, H.A.; Abdelbaset, M. Neuroprotective Effect of Crocus sativus against Cerebral Ischemia in Rats. *Metab. Brain Dis.* **2020**, *35*, 427–439, https://doi.org/10.1007/s11011-019-00492-3.
11. Gudarzi, S.; Jafari, M.; Pirzad Jahromi, G.; Eshrati, R.; Asadollahi, M.; Nikdokht, P. Evaluation of Modulatory Effects of Saffron (Crocus sativus L.) Aqueous Extract on Oxidative Stress in Ischemic Stroke Patients: A Randomized Clinical Trial. *Nutr. Neurosci.* **2022**, *25*, 1137–1146, https://doi.org/10.1080/1028415x.2020.1840118.
12. Yaidikar, L.; Byna, B.; Thakur, S.R. Neuroprotective Effect of Punicalagin against Cerebral Ischemia–Reperfusion-Induced Oxidative Brain Injury in Rats. *J. Stroke Cerebrovasc. Dis.* **2014**, *23*, 2869–2878, https://doi.org/10.1016/j.jstrokecerebrovasdis.2014.06.011.
13. Flores-Bazán, T.; Betanzos-Cabrera, G.; Guerrero-Solano, J.A.; Negrete-Díaz, J.V.; German-Ponciano, L.J.; Olivo-Ramírez, D. Pomegranate (Punica granatum L.) and Its Phytochemicals as Anxiolytic: An Underreported Effect with Therapeutic Potential—A Systematic Review. *Brain Res.* **2023**, *1820*, 148554, https://doi.org/10.1016/j.brainres.2023.148554.
14. Pujari, R.R.; Vyawahare, N.S.; Thakurdesai, P.A. Neuroprotective and Antioxidant Role of Phoenix dactylifera in Permanent Bilateral Common Carotid Occlusion in Rats. *J. Acute Dis.* **2014**, *3*, 104–114, https://doi.org/10.1016/S2221-6189(14)60026-3.
15. Asdaq, S.M.B.; Almutiri, A.A.; Alenzi, A.; Shaikh, M.; Shaik, M.A.; Alshehri, S.; Rabbani, S.I. Unveiling the Neuroprotective Potential of Date Palm (Phoenix dactylifera): A Systematic Review. *Pharmaceuticals* **2024**, *17*, 1221, https://doi.org/10.3390/ph17091221.
16. Tan, M.A.; Sharma, N.; An, S.S.A. Multi-Target Approach of Murraya koenigii Leaves in Treating Neurodegenerative Diseases. *Pharmaceuticals* **2022**, *15*, 188, https://doi.org/10.3390/ph15020188.
17. Norouzkhani, N.; Karimi, A.G.; Badami, N.; Jalalifar, E.; Mahmoudvand, B.; Ansari, A.; et al. From Kitchen to Clinic: Pharmacotherapeutic Potential of Common Spices in Indian Cooking in Age-Related Neurological Disorders. *Front. Pharmacol.* **2022**, *13*, 960037, https://doi.org/10.3389/fphar.2022.960037.
18. Elsayed, S.; El-Habeby, M.; El-Sherif, N.; Al-Gholam, M. Influence of Global Cerebral Ischemia/Reperfusion Injury on Rat Dentate Gyrus and the Possible Protective Effect of Beetroot (Beta vulgaris L.) Extract. *Eur. J. Anat.* **2021**, *25*, 389–402.
19. Mirahmadi, K.; Asgharzadeh, N.; Lorigooini, Z.; Mardani, M.; Rabiei, Z.; Shahrani, D.; et al. The Effect of Beet Leaf (Beta vulgaris) Extract on Learning and Memory after Cerebral Ischemic Reperfusion in Rats. *Future Nat. Prod.* **2024**, 10, 7–14, https://doi.org/10.34172/fnp.165.
20. Kashyap, I.; Deb, R.; Battineni, A.; Nagotu, S. Acyl-CoA Oxidase: From Its Expression, Structure, Folding, and Import to Its Role in Human Health and Disease. *Mol. Genet. Genom.* **2023**, *298*, 1247–1260, https://doi.org/10.1007/s00438-023-02059-5.
21. Morita, A.; Enokizono, T.; Ohto, T.; Tanaka, M.; Watanabe, S.; Takada, Y.; Iwama, K.; Mizuguchi, T.; Matsumoto, N.; Morita, M. Novel ACOX1 mutations in two siblings with peroxisomal acyl-CoA oxidase deficiency. *Brain and Development* **2021**, *43*, 475-481, https://doi.org/10.1016/j.braindev.2020.10.011.
22. Chung, H.-l.; Wangler, M.F.; Marcogliese, P.C.; Jo, J.; Ravenscroft, T.A.; Zuo, Z.; Duraine, L.; Sadeghzadeh, S.; Li-Kroeger, D.; Schmidt, R.E. Loss-or gain-of-function mutations in ACOX1 cause axonal loss via different mechanisms. *Neuron* **2020**, *106*, 589-606. e586, https://doi.org/10.1016/j.neuron.2020.02.021.
23. Szrok-Jurga, S.; Turyn, J.; Hebanowska, A.; Swierczynski, J.; Czumaj, A.; Sledzinski, T.; Stelmanska, E. The Role of Acyl-CoA β-Oxidation in Brain Metabolism and Neurodegenerative Diseases. *Int. J. Mol. Sci.* **2023**, 24, 13977, https://doi.org/10.3390/ijms241813977.
24. Qi, X.; Lin, H.; Hou, Y.; Su, X.; Gao, Y. Comprehensive analysis of potential miRNA-target mRNA-immunocyte subtype network in cerebral infarction. *Eur. Neurol.* **2022**, *85*, 148-161, https://doi.org/10.1159/000518893.
25. Shokr MM. Rewiring brain immunity: targeting microglial metabolism for neuroprotection in neurodegenerative disorders. Metab. Brain Dis. 2025;40(1):326. doi:10.1007/s11011-025-01739-y.
26. Dobrynina, L.A.; Makarova, A.G.; Shabalina, A.A.; Burmak, A.G.; Shlapakova, P.S.; Shamtieva, K.V.; Tsypushtanova, M.M.; Kremneva, E.I.; Zabitova, M.R.; Filatov, A.S. The role of changes in the expression

of inflammation-associated genes in the variants of cerebral small vessel disease. *Int. J. Mol. Sci.* **2024**, *25*, 8113, https://doi.org/10.3390/ijms25158113.
27. Jafarpour, S.; Khoshnood, M.; Santoro, J.D. Child Neurology: Neurodegenerative Encephalomyelopathy Associated with ACOX1 Gain-of-Function Variation Partially Responsive to Immunotherapy. *Neurology* **2022**, *99*, 341–346, https://doi.org/10.1212/WNL.0000000000200935.
28. Mohana Priya, R.; Irfan, N.; Mohammed Zaidh, S. Binding and dynamics of diferuloylmethane-pyrimidine with C-Met protein. *J. Indian Chem. Soc.* **2025**, *102*, 101849. https://doi.org/10.1016/j.jics.2025.101849.
29. Lu, Q.; Zong, W.; Zhang, M.; Chen, Z.; Yang, Z. The Overlooked Transformation Mechanisms of VLCFAs: Peroxisomal β-Oxidation. *Agriculture* **2022**, *12*, 947, https://doi.org/10.3390/agriculture12070947.
30. Kanehisa, M.; Furumichi, M.; Sato, Y.; Matsuura, Y.; Ishiguro-Watanabe, M. KEGG: Biological Systems Database as a Model of the Real World. *Nucl. Acids Res.* **2025**, *53*, D672–D677, https://doi.org/10.1093/nar/gkae909.
31. Zaidh, S.M.; Vengateswaran, H.T.; Habeeb, M.; Aher, K.B.; Bhavar, G.B.; Irfan, N.; Lakshmi, K. Network pharmacology and AI in cancer research uncovering biomarkers and therapeutic targets for RALGDS mutations. Sci. Rep. 2025, 15, 1-13, https://doi.org/10.1038/s41598-025-91568-x.
32. Zhang, P.; Zhang, D.; Zhou, W.; Wang, L.; Wang, B.; Zhang, T.; Li, S. Network Pharmacology: Towards the Artificial Intelligence-Based Precision Traditional Chinese Medicine. *Brief. Bioinform.* **2023**, *25*, bbad451, https://doi.org/10.1093/bib/bbad451.
33. Szklarczyk, D.; Kirsch, R.; Koutrouli, M.; Nastou, K.; Mehryary, F.; Hachilif, R.; Gable, A.L.; Fang, T.; Doncheva, N.T.; Pyysalo, S. The STRING database in 2023: protein–protein association networks and functional enrichment analyses for any sequenced genome of interest. *Nucl. Acids Res.* **2023**, *51*, D638-D646, https://doi.org/10.1093/nar/gkac1000.
34. Priya, R.M.; Zaidh, S.M.; Navabshan, I.; Venkataraman, S.; Ahmed, H.N.; Ismail, Y. Pharmacophore-based SAR Analysis and Synthetic Route Review of Imidazole Core Analogues. *Curr. Appl. Sci. Technol.* **2025**, *25*, e0261082-e0261082, https://doi.org/10.55003/cast.2024.261082.
35. Madhavi Sastry, G.; Adzhigirey, M.; Day, T.; Annabhimoju, R.; Sherman, W. Protein and Ligand Preparation: Parameters, Protocols, and Influence on Virtual Screening Enrichments. *J. Comput. Aided Mol. Des.* **2013**, 27, 221–234, https://doi.org/10.1007/s10822-013-9644-8.
36. Irfan, N.; Vaithyanathan, P.; Anandaram, H.; Mohammed Zaidh, S.; Priya Varshini, S.; Puratchikody, A. Active and Allosteric Site Binding MM-QM Studies of Methylidene Tetracyclo Derivative in PCSK9 Protein Intended to Make a Safe Antilipidemic Agent. *J. Biomol. Struct. Dyn.* **2023**, *42*, 6813-6822, https://doi.org/10.1080/07391102.2023.2239928.
37. Mohammed Zaidh, S.; Aher, K.B.; Bhavar, G.B.; Irfan, N.; Ahmed, H.N.; Ismail, Y. Genes Adaptability and NOL6 Protein Inhibition Studies of Fabricated Flavan-3-ols Lead Skeleton Intended to Treat Breast Carcinoma. International Journal of Biological *Macromolecules* **2023**, *258*, 127661, https://doi.org/10.1016/j.ijbiomac.2023.127661.
38. Maraf, M.B.; Mountessou, B.Y.G.; Merlin, T.F.H.; Ariane, P.; Fekoua, J.N.N.; Yves, T.B.J.; Raoul, T.T.D.; Zintchem, A.A.A.; Bebga, G.; Mbouombouo, N.I. Virtual screening, MMGBSA, and molecular dynamics approaches for identification of natural products from South African biodiversity as potential Onchocerca volvulus pi-class glutathione S-transferase inhibitors. *Heliyon* **2024**, *10*, e29560, https://doi.org/10.1016/j.heliyon.2024.e29560.
39. Jiang, X.; Li, S.; Zhang, H.; Wang, L.L. Discovery of Potentially Biased Agonists of Mu-Opioid Receptor (MOR) through Molecular Docking, Pharmacophore Modeling, and MD Simulation. *Comput. Biol. Chem.* **2021**, *90*, 107405, https://doi.org/10.1016/j.compbiolchem.2020.107405.
40. Ferreira, L.; dos Santos, R.; Oliva, G.; Andricopulo, A. Molecular Docking and Structure-Based Drug Design Strategies. *Molecules* **2015**, *20*, 13384–13421, https://doi.org/10.3390/molecules200713384.
41. Garkusha, N.A.; Anikeeva, O.P.; Bayıl, I.; Taskin-Tok, T.; Safin, D.A. DFT, ADMET, Molecular Docking and Molecular Dynamics Studies of Pyridoxal. *J. Indian Chem. Soc.* **2023**, *100*, 100926, https://doi.org/10.1016/j.jics.2023.100926.
42. Bratek, E.; Ziembowicz, A.; Bronisz, A.; Salinska, E. The Activation of Group II Metabotropic Glutamate Receptors Protects Neonatal Rat Brains from Oxidative Stress Injury after Hypoxia-Ischemia. *PLoS ONE* **2018**, *13*, e0200933, https://doi.org/10.1371/journal.pone.0200933.
43. Ferrari, F.; Gorini, A.; Hoyer, S.; Villa, R.F. Glutamate Metabolism in Cerebral Mitochondria after Ischemia and Post-Ischemic Recovery during Aging: Relationships with Brain Energy Metabolism. *J. Neurochem.* **2018**, *146*, 416–428, https://doi.org/10.1111/jnc.14464.

44. Belov Kirdajova, D.; Kriska, J.; Tureckova, J.; Anderova, M. Ischemia-Triggered Glutamate Excitotoxicity from the Perspective of Glial Cells. *Front. Cell. Neurosci.* **2020**, *14*, 51, https://doi.org/10.3389/fncel.2020.00051.
45. Fidaleo, M.; Fanelli, F.; Ceru, M.P.; Moreno, S. Neuroprotective Properties of Peroxisome Proliferator-Activated Receptor Alpha (PPARα) and Its Lipid Ligands. *Curr. Med. Chem.* **2014**, *21*, 2803–2828, https://doi.org/10.2174/09298673216661403031434555.
46. Moreno-López, B.; Romero-Grimaldi, C.; Noval, J.A.; Murillo-Carretero, M.; Matarredona, E.R.; Estrada, C. Nitric Oxide Is a Physiological Inhibitor of Neurogenesis in the Adult Mouse Subventricular Zone and Olfactory Bulb. *J. Neurosci.* **2004**, *24*, 85–95, https://doi.org/10.1523/JNEUROSCI.1574-03.2004.
47. Trompier, D.; Vejux, A.; Zarrouk, A.; Gondcaille, C.; Geillon, F.; Nury, T.; Savary, S.; Lizard, G. Brain peroxisomes. *Biochimie* **2014**, *98*, 102-110, https://doi.org/10.1016/j.biochi.2013.09.009.
48. Tawbeh, A.; Gondcaille, C.; Saih, F.-E.; Raas, Q.; Loichot, D.; Hamon, Y.; Keime, C.; Benani, A.; Di Cara, F.; Cherkaoui-Malki, M. Impaired peroxisomal beta-oxidation in microglia triggers oxidative stress and impacts neurons and oligodendrocytes. *Front. Mol. Neurosci.* **2025**, *18*, 1542938, https://doi.org/10.3389/fnmol.2025.1542938.
49. Liao, W.; Wen, Y.; Yang, S.; Duan, Y.; Liu, Z. Research Progress and Perspectives of N-Methyl-D-Aspartate Receptor in Myocardial and Cerebral Ischemia-Reperfusion Injury: A Review. *Medicine* **2023**, *102*, e35490, https://doi.org/10.1097/MD.0000000000035490.
50. Zhang, F.; Guo, A.; Liu, C.; Comb, M.; Hu, B. Phosphorylation and Assembly of Glutamate Receptors after Brain Ischemia. *Stroke* **2013**, *44*, 170–176, https://doi.org/10.1161/strokeaha.112.667253.
51. Shi, B.; Chen, J.; Guo, H.; Shi, X.; Tai, Q.; Chen, G.; Yao, H.; Mi, X.; Zhong, R.; Lu, Y. ACOX1 activates autophagy via the ROS/mTOR pathway to suppress proliferation and migration of colorectal cancer. *Sci. Rep.* **2025**, *15*, 2992, https://doi.org/10.1038/s41598-025-87728-8.
52. You, L.; Chen, J.; Liu, W.; Xiang, Q.; Luo, Z.; Wang, W.; Xu, W.; Wu, K.; Zhang, Q.; Liu, Y. Enterovirus 71 induces neural cell apoptosis and autophagy through promoting ACOX1 downregulation and ROS generation. *Virulence* **2020**, *11*, 537-553, https://doi.org/10.1080/21505594.2020.1766790.
53. Changes in lipid metabolism track with the progression of neurofibrillary pathology in tauopathies.J. Neuroinflammation. 2024;21:78. doi:10.1186/s12974-024-03060-4..
54. Kim, J.-T.; Won, S.Y.; Kang, K.; Kim, S.-H.; Park, M.-S.; Choi, K.-H.; Nam, T.-S.; Denis, S.W.; Ferdinandusse, S.; Lee, J.E. ACOX3 dysfunction as a potential cause of recurrent spontaneous vasospasm of internal carotid artery. *Transl. Stroke Res.* **2020**, *11*, 1041-1051, https://doi.org/10.1007/s12975-020-00779-z.
55. Hu, Y.; Gu, J.; Jin, X.; Wu, X.; Li, H.; Bai, L.; Wu, J.; Li Sr, X. Asiatic acid alleviates subarachnoid hemorrhage-induced brain injury in rats by inhibiting ferroptosis of neurons via targeting acyl-coenzyme a oxidase 1. *Neuropharmacology* **2025**, *262*, 110208, https://doi.org/10.1016/j.neuropharm.2024.110208.
56. El Rhabori, S.; El Aissouq, A.; Daoui, O.; Elkhattabi, S.; Chtita, S.; Khalil, F. Design of New Molecules against Cervical Cancer Using DFT, Theoretical Spectroscopy, 2D/3D-QSAR, Molecular Docking, Pharmacophore and ADMET Investigations. *Heliyon* **2024**, *10*, e24551, https://doi.org/10.1016/j.heliyon.2024.e24551.
57. Pu, F.; Mishima, K.; Irie, K.; Motohashi, K.; Tanaka, Y.; Orito, K.; Egawa, T.; Kitamura, Y.; Egashira, N.; Iwasaki, K. Neuroprotective effects of quercetin and rutin on spatial memory impairment in an 8-arm radial maze task and neuronal death induced by repeated cerebral ischemia in rats. *J. Pharmacol. Sci.* **2007**, 104, 329-334, https://doi.org/10.1254/jphs.FP0070247.

Publisher's Note & Disclaimer